

# The Geometry of Niggli Reduction I: The Boundary Polytopes of the Niggli Cone

LAWRENCE C. ANDREWS<sup>1</sup> AND HERBERT J. BERNSTEIN<sup>2,\*</sup>

<sup>1</sup>*Micro Encoder Inc., 11533 NE 118th St, #200, Kirkland, WA 98034-7111 USA*

<sup>2</sup>*Dowling College, 1300 William Floyd Parkway, Shirley, NY 11967 USA*

\**To whom correspondence should be addressed. Email: yaya@dowling.edu*

August 12, 2013

## Abstract

Correct identification of the Bravais lattice of a crystal is an important early step in structure solution. Niggli reduction is a commonly used technique. We investigate the boundary polytopes of the Niggli-reduced cone  $\mathcal{N}$  in the six-dimensional space  $\mathbf{G}^6$  by algebraic analysis and organized random probing of regions near 1-, 2-, 3-, 4-, 5-, 6-, 7- and 8-fold boundary polytope intersections. We limit our consideration of valid boundary polytopes to those avoiding the mathematically interesting but crystallographically impossible cases of zero length cell edges. Combinations of boundary polytopes without a valid intersection in the closure of the Niggli cone or with an intersection that would force a cell edge to zero or without neighboring probe points are eliminated. 216 boundary polytopes are found. There are 15 5-D boundary polytopes of the full  $\mathbf{G}^6$  Niggli cone  $\mathcal{N}$ , 53 4-D boundary polytopes resulting from intersections of pairs of the 15 5-D boundary polytopes, 79 3-D boundary polytopes resulting from 2-fold, 3-fold and 4-fold intersections of the 15 5-D boundary polytopes, 55 2-D boundary polytopes resulting from 2-fold, 3-fold, 4-fold and higher intersections of the 15 5-D boundary polytopes, 14 1-D boundary polytopes resulting from 3-fold and higher intersections of the 15 5-D boundary polytopes.

All of the primitive lattice types can be represented as combinations of the 15 5-D boundary polytopes. All of the non-primitive lattice types can be represented as combinations of the 15 5-D boundary polytopes and of the 7 special-position subspaces of the 5-D boundary polytopes. This study provides a new, simpler and arguably more intuitive basis set for the classification of lattice characters and helps to illuminate some of the complexities in Bravais lattice identification. The classification is intended to help in organizing database searches and in understanding which lattice symmetries are “close” to a given experimentally determined cell.

## 1 Introduction

This is the first in a series of papers on understanding and classifying crystallographic lattices and the cell parameters commonly used to identify those lattices. This paper is concerned with fundamental mathematical issues underlying the subsequent papers. The next two papers are concerned with the application of this approach to lattice identification [4] and to unit cell databases [18]. More papers based on this formalism are in preparation. The boundary and matrix definitions from this paper are needed for a full understanding of the subsequent papers.

The wide-spread use of Niggli reduction in crystallography implies that it should be thoroughly understood. Robust identification of Bravais lattices and lookup of unit cell parameters in databases would be improved if a successful embedding of the Niggli space could be achieved. An essential preliminary step towards doing such an embedding is the mapping of the boundaries of the space of Niggli-reduced cells.

Failure to correctly identify the Bravais lattice of a crystal can compromise subsequent least-squares calculations or even the solution of a structure. There are two commonly used ways to obtain a unique representative of the infinite number of cells that may be used to generate a given lattice: Niggli reduction [20] and Delaunay reduction [10]. We follow the conventions of the International Tables for Crystallography [8] in basing this paper on Niggli reduction, and we will recast the discussion in terms of Delaunay reduction in a future study. Niggli reduction defines a complex space that has not previously been fully analyzed. Several authors have published interesting commentaries on the properties of this space [15] [21] [12]. These studies use the space  $\mathbf{G}^6$  [3], or a similar metric-tensor-based space, or a projection of  $\mathbf{G}^6$  to a space of lower dimensionality, respectively. Two principal uses of Niggli reduction are the determination of Bravais lattice type and the construction of databases using a representation of the unit cell for the key [2] [26] [9].

Given a precisely determined reduced cell, the lattice symmetry may be unambiguously inferred. In addition, reduced cells are useful in searching for sub- and super-cells, indexing of powder patterns and in twinned crystal studies. Without a suitable metric and a clear understanding of the geometry of the boundaries of the space, searches of lattices in the neighborhood of a given cell must either be excessively broad and produce many false positives, or, if made tighter, risk missing important candidates, especially in the vicinity of 90 degree angles.

As noted in [5] the concept of a reduced cell is strongly related to the concept of a reduced ternary quadratic form [23] [24]. Reduced cells have become an important computational tool in crystallography (just as reduced quadratic forms are an important tool in computational number theory) but much of the literature focuses on an essentially qualitative approach, taking a reduced cell as an absolute indicator of symmetry and not considering the impact of experimental error [3]. Consideration of experimental error requires use of a distance metric dealing with reduced cells. Such metrics have been used in a 6-dimensional approach [27], another 6-dimensional approach [3], a B-matrix approach [17] and a “distortion index” approach [19].

In addition, because the processes of both Niggli and Delaunay reduction can produce large discontinuities in reduced cell parameters from small changes in the lattice, an effective use of a metric must allow for such discontinuities, either by a combinatorial search or by a metric-preserving embedding in a higher dimensional space that removes the discontinuities. Until now, crystallographic software appears either to have used a demanding combinatorial approach or simply to have given up on a doing complete search. The purpose of this paper is to take the necessary first steps towards adding an embedding to the existing combinatorial approaches by clearly mapping the boundary discontinuities and their related transformations.

There have been multiple investigations of such boundaries, albeit without a consideration of experimental error in most cases. See, for example, Gruber [12] [13] for a review and an approach using a 5-dimensional space based on the metric tensor. Gruber’s 1997 approach partitions the space of reduced cells into 127 disjoint components (genera), based on 67 1- to 4-dimensional “hyperfaces” further subdivided into 227 hyperfaces in order to achieve a common partitioning applicable to both Niggli and Delaunay reduction. Unfortunately, Gruber’s reduction to 5 dimensions, and any purely topological approach without a metric that allows error propagation from the experimental data, makes it difficult or impossible to do a full perturbation analysis of the impact of experimental errors.

Therefore in this investigation we return to the full 6-dimensional space [3],  $\mathbf{G}^6$ , of unit cells

based on the metric tensor and use algebraic techniques confirmed by a Monte Carlo technique to explore the “natural” 5-, 4-, 3-, 2- and 1-dimensional boundary polytopes of the 6-dimensional polytope of Niggli-reduced cells. The two techniques are mutual supportive. The lower dimensional boundaries are an algebraic consequence of the 5-dimensional boundaries. The lower dimensional boundaries derived algebraically are confirmed by the Monte Carlo technique which helps to identify unpopulated boundaries and boundaries that drop to lower dimension due to glancing intersections with multiple other boundaries.

There are 15 5-dimensional boundary polytopes and a total of 216 boundary polytopes. In this approach, all the boundary polytopes are on the surface of the closure of the 6-dimensional Niggli-reduced polytope. Identification of these boundary polytopes and the reduction transformations to be applied in crossing them is an essential step in either a combinatorial error analysis or in embedding  $\mathbf{G}^6$  into a higher dimensional space for an analytic error analysis, and it is useful for database searches.

The 15 5-D boundary polytopes give the complete shape of the space of Niggli-reduced cells. All of the primitive lattice types can be represented as combinations of the 15 5-D boundary polytopes. All of the non-primitive lattice types can be represented as combinations of the 15 5-D boundary polytopes and of the 7 special-position subspaces of the 5-D boundary polytopes. By confining our attention to just the Niggli reduction, the result is a simpler classification than Gruber’s with more direct applicability to an embedding and database searching. The embedding and database searches are the subjects of following studies.

## 2 The space $\mathbf{G}^6$

$\mathbf{G}^6$  is a reformulation of the crystallographic metric tensor and the “Niggli matrix” (itself a reformulation of the metric tensor) [3]. A vector  $\vec{g}$  in  $\mathbf{G}^6$  is defined as:

$$\begin{aligned} \vec{g} &= \left( \vec{a} \cdot \vec{a}, \vec{b} \cdot \vec{b}, \vec{c} \cdot \vec{c}, 2\vec{b} \cdot \vec{c}, 2\vec{a} \cdot \vec{c}, 2\vec{a} \cdot \vec{b} \right) \\ &= \left( \|\vec{a}\|^2, \|\vec{b}\|^2, \|\vec{c}\|^2, 2\|\vec{b}\|\|\vec{c}\|\cos(\alpha), \right. \\ &\quad \left. 2\|\vec{a}\|\|\vec{c}\|\cos(\beta), 2\|\vec{a}\|\|\vec{b}\|\cos(\gamma) \right) \\ &= (g_1, g_2, g_3, g_4, g_5, g_6) = g_{\{1,2,3\}}, g_{\{4,5,6\}} \end{aligned}$$

where  $\vec{a}$ ,  $\vec{b}$ ,  $\vec{c}$  are the unit cell edge vectors, and “.” indicates the dot product. The unit cell is chosen to be primitive.

The notation  $g_{\{4,5,6\}}$  is used to denote the elements  $(g_4, g_5, g_6)$  from the full  $\mathbf{G}^6$  vector.

## 3 The Niggli Conditions

The Niggli-reduced cell of a lattice is a unique choice from among the infinite number of alternate cells that generate the same lattice [20]. A Buerger-reduced cell for a given lattice is any cell that generates that lattice, chosen such that no other cell has shorter cell edges [7]. Even after allowing for the equivalence of cells in which the directions of axes are reversed or axes of the same length are exchanged, there can be up to five alternate Buerger-reduced cells for the same lattice [11]. The Niggli conditions allow the selection of a unique reduced cell for a given lattice from among the alternate Buerger reduced cells for that lattice.

Niggli reduction consists of converting the original cell to a primitive one and then alternately applying two operations: conversion to standard presentation and reduction [20] [3, Table 1].

The convention for meeting the combined Buerger and Niggli conditions is based on increasingly restrictive layers of constraints:

If  $g_1 < g_2 < g_3$ ,  $|g_4| < g_2$ ,  $|g_5| < g_1$ ,  $|g_6| < g_1$  and either  $g_{\{4,5,6\}} > 0$  or  $g_{\{4,5,6\}} \leq 0$  then we have a Niggli-reduced cell, and we are done.

The remaining conditions are imposed when any of the above inequalities becomes an equality or the elements of  $g_{\{4,5,6\}}$  are not consistently all strictly positive or are not consistently all less than or equal to zero.

The full set of combined Buerger and Niggli conditions in addition to those for the cell edge lengths being minimal is:

$$\text{require } 0 \leq g_1 \leq g_2 \leq g_3$$

$$\text{if } g_1 = g_2, \text{ then require } |g_4| \leq |g_5| \tag{3.1}$$

$$\text{if } g_2 = g_3, \text{ then require } |g_5| \leq |g_6| \tag{3.2}$$

$$\text{require } \{g_4 > 0 \text{ and } g_5 > 0 \text{ and } g_6 > 0\}$$

$$\text{or require } \{g_4 \leq 0 \text{ and } g_5 \leq 0 \text{ and } g_6 \leq 0\}$$

$$\text{require } |g_4| \leq g_2$$

$$\text{require } |g_5| \leq g_1$$

$$\text{require } |g_6| \leq g_1$$

$$\text{require } g_3 \leq g_1 + g_2 + g_3 + g_4 + g_5 + g_6$$

$$\text{if } g_4 = g_2, \text{ then require } g_6 \leq 2g_5 \tag{3.3}$$

$$\text{if } g_5 = g_1, \text{ then require } g_6 \leq 2g_4$$

$$\text{if } g_6 = g_1, \text{ then require } g_5 \leq 2g_4$$

$$\text{if } g_4 = -g_2, \text{ then require } g_6 = 0$$

$$\text{if } g_5 = -g_1, \text{ then require } g_6 = 0$$

$$\text{if } g_6 = -g_1, \text{ then require } g_5 = 0 \tag{3.4}$$

$$\text{if } g_3 = g_1 + g_2 + g_3 + g_4 + g_5 + g_6, \text{ then require } 2g_1 + 2g_5 + g_6 \leq 0$$

The  $\mathbf{G}^6$  transformations associated with each of these steps are enumerated in [3]. Application of these operations must be repeated until all are satisfied.

## 4 Notation and Boundary Polytopes

We define the manifold of Niggli reduced cells in  $\mathbf{G}^6$  as  $\mathbf{N}$  and refer to it as the “Niggli cone”.

The interior of  $\mathbf{N}$ ,  $int(\mathbf{N})$ , is defined as the set of  $\vec{n} \in \mathbf{N}$  such that there exists  $r > 0$  such that for all  $\vec{g} \in \mathbf{G}^6$  such that  $\|\vec{g} - \vec{n}\| < r$ ,  $\vec{g} \in \mathbf{N}$ .

The closure of  $\mathbf{N}$ ,  $cl(\mathbf{N})$ , is defined as the set of  $\vec{g} \in \mathbf{G}^6$  such that for all  $r > 0$  there exists  $\vec{n} \in \mathbf{N}$  such that  $\|\vec{g} - \vec{n}\| \leq r$ .

The boundary of  $\mathbf{N}$ ,  $\partial(\mathbf{N})$ , is defined as the set of points in  $cl(\mathbf{N})$  not in  $int(\mathbf{N})$ .

The boundary of  $\mathbf{N}$  is created by the linear constraints of Niggli reduction and therefore can be decomposed into the union of “polytopes,” *i.e.* flat facets with straight edges.

We distinguish the primary boundary polytopes from their edges, which are also polytopes, by “dimension” which is the number of vectors in a basis for the interior of the polytope.

$\mathbf{N}$  is a six-dimensional (6-D) polytope.  $\mathbf{N}$  is a double-ended cone-like region going through the origin to infinity in both directions. The boundary polytopes are flat facets created by the intersections of hyperplanes through the origin. The boundary polytopes are, of course, of lower-dimension than  $\mathbf{N}$ . Therefore any randomly selected vector in  $\mathbf{G}^6$  has a vanishingly small probability of occupying any particular 5-dimensional (“5-D”) boundary polytope, and it has an even lower probability of occupying one of the lower-dimensional boundary polytopes resulting from the intersections of 5-D boundary polytopes. Some boundary polytopes are “open”, *i.e.* while there are Niggli-reduced cells near that boundary, some or all of the points on those boundary polytopes are not themselves Niggli-reduced.

Our task is to identify the 5-D boundary polytopes that give  $\mathbf{N}$  its shape. Those 5-D boundaries and the transforms involved in crossing them generate all the rest of the structure. However, in order to understand the shape of a given 5-D boundary polytope, we need the 4-D edges that bound it. In order to understand the shape of a given 4-D boundary polytope, we need the 3-D edges that bound it. In order to understand the shape of a given 3-D boundary polytope, we need the 2-D edges that bound it. In order to understand the shape of a given 2-D boundary polytope, we need the 1-D edges that bound it. From this classification we gain a better understanding of the relationships among Bravais lattice types, and, perhaps more importantly, this provides essential information needed to organize computations. Hosoya [14] addressed a different, but related, classification. We discuss the relationship between boundary polytope identification, lattice types and Hosoya’s approach in section 11. Hosoya recognized the complexity of boundary identifications for  $\mathbf{N}$  and introduced the use of Monte Carlo searching to clarify the relationships. We apply a Monte Carlo search in Appendix A.

The reduction steps convert a non-reduced cell into one that has at least one edge shorter than the starting edges, and other steps in the case of equality convert a non-reduced cell into a cell that is more orthogonal than the starting cell. These operations are accomplished by choosing a face- or body-diagonal to replace one of the cell edges. The conditions added to remove the ambiguities in the case of equalities allow for a unique choice of Niggli cell in all cases but thereby create complex boundary conditions [3]. For example, the cell edge equalities in equations (3.1) and (3.2) create boundary polytopes across which elements of both  $g_{\{1,2,3\}}$  and of  $g_{\{4,5,6\}}$  are exchanged, while equations (3.3) through (3.4) create boundary polytopes across which edges are exchanged for face-diagonals.

A boundary polytope does not necessarily consist entirely of Niggli-reduced cells, but must be “near” Niggli-reduced cells and must be “near” non-Niggli-reduced cells as well. We define a boundary polytope,  $\mathbf{F} \subseteq \mathbf{N}$  as a subset of  $\mathbf{N}$  for which there is an associated matrix  $M_{\mathbf{F}}$  such that for all points  $\vec{\gamma} \in \mathbf{F}$  there exists  $\delta > 0$  such that for all  $\vec{n} \notin \mathbf{N}$  where  $\|\vec{n} - \vec{\gamma}\| < \delta$ ,  $M_{\mathbf{F}}(\vec{\gamma}) \in \mathbf{N}$ . Each boundary polytope is a portion of the boundary for which there is a single transformation matrix that maps the nearby non-Niggli-reduced cells to Niggli-reduced

cells. This is not necessarily a mapping back to the starting point, not even to a point near the starting point, not even for points on the boundary polytope itself. We look for point-by-point invariance in defining special-position subspaces in section 5.

Each boundary polytope  $\Gamma$  has an associated “projector”  $P_\Gamma$ , which is the linear transformation that maps an arbitrary  $g \in \mathbf{G}^6$  to the point  $P_\Gamma g$  closest to  $g$  in the hyperplane containing  $\Gamma$ . It is important to understand that  $P_\Gamma g$  may not be Niggli reduced, nor even close to the Niggli cone.

## 5 Special-Position Subspaces

In an analysis of symmetry, special positions play an important role. A special position is a point invariant under a symmetry transformation, an eigenvector, of eigenvalue 1, of the transformation. We define a special-position subspace of a boundary polytope,  $\Gamma$ , as the intersection of the eigenspace of eigenvalue 1 of  $M_\Gamma$  with the boundary polytope. Formally, for a boundary polytope,  $\Gamma$ , with associated transformation matrix,  $M_\Gamma$ , the special-position subspace  $\Lambda(\Gamma, M_\Gamma)$  is defined as the set of points  $\vec{\gamma} \in \Gamma$  such that  $M_\Gamma(\vec{\gamma}) = \vec{\gamma}$ . In the case of boundary polytopes associated with a transformation matrix that goes from the all acute + + + case to the all obtuse – – – case or vice versa, there cannot be any Niggli-reduced special-position subspace, because the axial planes of the  $g_{\{4,5,6\}}$  subspace are excluded from the all acute + + + case. As we will see, while the special-position subspaces of the boundary polytopes are not needed in order to classify the primitive lattice types, they come into play in classifying the non-primitive lattice types.

If we have two boundary polytopes  $\Gamma_1, \Gamma_2 \subset N$ , we denote the intersection of the closure of  $\Gamma_1$  and the closure of  $\Gamma_2$  as  $\Gamma_1\Gamma_2$ . Note that intersection is a commutative operation, *i.e.*  $\Gamma_1\Gamma_2 = \Gamma_2\Gamma_1$ .

Because we have restricted the boundary polytope in this paper to have only one associated matrix, we use the notation  $\hat{\Gamma}$  for  $\Lambda(\Gamma, M_\Gamma)$ . In general, an infinite number of higher dimensional polytopes will intersect  $\Gamma$  in  $\hat{\Gamma}$ . We distinguish such a higher dimensional polytope as  $\Gamma'$ . Thus  $\Gamma\Gamma' = \hat{\Gamma}$ .

## 6 The fifteen 5-D boundary polytopes

The fifteen 5-dimensional boundary polytopes and their special-position subspaces may be organized as shown in Table 1, in which we use the hexadecimal digits 1 through F as identifiers. For each 5-dimensional boundary polytope  $\Gamma$  in Table 1 having a non-trivial special-position subspace, we designate the particular choice of higher dimensional polytope intersecting  $\Gamma$  in  $\hat{\Gamma}$  as  $\Gamma'$ . See section 6.0.3 for a concrete example.

In the discussions of the fifteen 5-dimensional boundary polytopes, below, we give the condition being satisfied, the right-handed  $\mathbf{E}^3$  presentation of the boundary transformation cell-edge-by-cell-edge, a  $\mathbf{G}^6$  matrix presentation of the same boundary transformation and a  $\mathbf{G}^6$  matrix presentation of a projector into the hyperplane of that boundary. Note that both a right-handed  $\mathbf{E}^3$  presentation and its negative (left-handed) presentation would map into the same  $\mathbf{G}^6$  presentation.

### 6.0.1 Equal cell-edge cases:

Cases 1 and 2 arise when two cell edges have equal length. The conditions of Niggli reduction impose a secondary condition on the associated angles for those two edges that resolves the

ambiguity in ordering them. For example, in case 1,  $\|\vec{a}\| = \|\vec{b}\|$  ( $g_1 = g_2$ ) and the Niggli-reduced  $\mathbf{G}^6$  vector  $U = (\mathbf{g}_1, \mathbf{g}_2, g_3, \mathbf{g}_4, \mathbf{g}_5, g_6)$  produces the same lattice as  $V = (\mathbf{g}_2, \mathbf{g}_1, g_3, \mathbf{g}_5, \mathbf{g}_4, g_6)$ , which is not Niggli-reduced if  $g_4$  and  $g_5$  have different values. In going from Niggli-reduced cells near  $U$  to Niggli-reduced cells near  $V$  (e.g. by decreasing  $g_2$  slightly), we are crossing a boundary polytope with a discontinuity in each of  $g_4$  and  $g_5$  [3]. We may represent the transformation that takes  $U$  into  $V$  at the first boundary polytope by the matrix  $M_1$  that maps  $U$  into  $V$  and the projector  $P_1$  that maps any  $\mathbf{G}^6$  vector into the  $g_1 = g_2$  boundary polytope.

$$\text{Case 1: } g_1 = g_2, \quad \vec{a} \rightarrow -\vec{b}, \quad \vec{b} \rightarrow -\vec{a}, \quad \vec{c} \rightarrow -\vec{c}$$

$$M_1 = (010000/100000/001000/000010/000100/000001)$$

$$P_1 = \left( \frac{1}{2} \frac{1}{2} 0000 / \frac{1}{2} \frac{1}{2} 0000 / 001000 / 000100 / 000010 / 000001 \right)$$

$$\mathbf{G}^6 \text{ subspace: } (r, r, s, t, u, v)$$

Similarly, for case 2,  $\|\vec{b}\| = \|\vec{c}\|$  ( $g_2 = g_3$ ),  $g_5$  and  $g_6$  are exchanged, yielding

$$\text{Case 2: } g_2 = g_3, \quad \vec{a} \rightarrow -\vec{a}, \quad \vec{b} \rightarrow -\vec{c}, \quad \vec{c} \rightarrow -\vec{b}$$

$$M_2 = (100000/001000/010000/000100/000001/000010)$$

$$P_2 = \left( 100000/0 \frac{1}{2} \frac{1}{2} 000 / 0 \frac{1}{2} \frac{1}{2} 000 / 000100 / 000010 / 000001 \right)$$

$$\mathbf{G}^6 \text{ subspace: } (r, s, s, t, u, v)$$

The remaining cell-edge case in which  $\|\vec{a}\| = \|\vec{c}\|$  ( $g_1 = g_3$ ), is only considered under Niggli reduction when  $\|\vec{a}\| = \|\vec{b}\|$  and  $\|\vec{b}\| = \|\vec{c}\|$  which is a combination of case 1 and case 2. This requires two simultaneous 5-dimensional constraints, thereby making  $g_1 = g_3$  a 4-dimensional rather than a 5-dimensional case.

The special-position subspaces  $\hat{1}$  and  $\hat{2}$  are obtained by adding the constraints  $1'$ :  $\{g_4 = g_5\}$  and  $2'$ :  $\{g_5 = g_6\}$ , respectively.

### 6.0.2 Ninety-degree cases:

Cases 3, 4 and 5 arise when a reduced-cell angle is ninety degrees. In those cases, the remaining cell angles both can be replaced by their supplements. This changes the sign of  $g_{\{4,5,6\}}$ .

$$\text{Case 3: } g_4 = 0, \quad \vec{a} \rightarrow \vec{a}, \quad \vec{b} \rightarrow -\vec{b}, \quad \vec{c} \rightarrow -\vec{c}$$

$$M_3 = (100000/010000/001000/000100/0000\bar{1}0/00000\bar{1})$$

$$P_3 = (100000/010000/001000/000000/000010/000001)$$

$$\mathbf{G}^6 \text{ subspace: } (r, s, t, 0, -u, -v)$$

$$\text{Case 4: } g_5 = 0, \quad \vec{a} \rightarrow -\vec{a}, \quad \vec{b} \rightarrow \vec{b}, \quad \vec{c} \rightarrow -\vec{c}$$

$$M_4 = (100000/010000/001000/000\bar{1}00/000010/00000\bar{1})$$

$$P_4 = (100000/010000/001000/000100/000000/000001)$$

$\mathbf{G}^6$  subspace:  $(r, s, t, -u, 0, -v)$

Case 5:  $g_6 = 0$ ,  $\vec{a} \rightarrow -\vec{a}$ ,  $\vec{b} \rightarrow -\vec{b}$ ,  $\vec{c} \rightarrow \vec{c}$

$$M_5 = (100000/010000/001000/000\bar{1}00/0000\bar{1}0/000001)$$

$$P_5 = (100000/010000/001000/000100/000010/000000)$$

$\mathbf{G}^6$  subspace:  $(r, s, t, -u, -v, 0)$

In each ninety-degree case, the special-position subspace consists of  $\hat{3}, \hat{4}, \hat{5}: \{g_4 = g_5 = g_6 = 0\}$ , *i.e.* the primitive orthorhombic case, and we take  $3': \{g_5 = g_6 = 0\}$ ,  $4': \{g_4 = g_6 = 0\}$ ,  $5': \{g_4 = g_5 = 0\}$ .

### 6.0.3 Face-diagonal cases:

Cases 6 through E are all face-diagonal cases, in which a cell edge is equal in length to a face-diagonal. Some complexity arises in the analysis because, unlike Delaunay reduction, Niggli reduction permits non-obtuse angles. We can always change the sign of any two elements of  $g_{\{4,5,6\}}$  by changing the direction of the cell edge involved with those two elements. For example, if we transform  $\vec{a}$  to  $-\vec{a}$  then, while  $g_1$  remains unaffected, the signs of each of  $g_5 = 2\vec{a} \cdot \vec{c}$  and  $g_6 = 2\vec{a} \cdot \vec{b}$  will change. Thus we can transform a cell having three acute angles to a cell having one acute angle and two obtuse angles, and we can transform a cell having three obtuse angles to a cell having one obtuse angle and two acute angles. The complete list of possible sign changes in  $g_{\{4,5,6\}}$  by changing the directions of axes are:

$$\begin{aligned} \{+++ \} &\Leftrightarrow \{- - + \} \Leftrightarrow \{- + - \} \Leftrightarrow \{+ - - \} \\ \{- - - \} &\Leftrightarrow \{+ + - \} \Leftrightarrow \{+ - + \} \Leftrightarrow \{- + + \} \end{aligned}$$

Unless one of the angles is ninety degrees (which introduces a zero into  $g_{\{4,5,6\}}$ ), we cannot ordinarily transform a Niggli-reduced cell with all-acute angles to one with all-obtuse angles by changing the directions of axes, nor can we transform a Niggli-reduced cell with all-obtuse angles to one with all-acute angles by changing the directions of the axes. Note that changing the direction of all three axes has no effect because all the sign changes cancel.

The face-diagonal cases do include cases in which transformations from, for example,  $+++$  to  $---$  do occur. Let us look in detail at cases 6 and 7,  $g_2 = g_4$ .

$$\begin{aligned} g_2 &= g_4 \\ g_2 - g_4 &= 0 \\ g_2 - g_4 + g_3 &= g_3 \\ \vec{b} \cdot \vec{b} - 2\vec{b} \cdot \vec{c} + \vec{c} \cdot \vec{c} &= \vec{c} \cdot \vec{c} \\ \|\vec{b} - \vec{c}\|^2 &= \|\vec{c}\|^2 \\ \|\vec{b} - \vec{c}\| &= \|\vec{c}\| \end{aligned}$$



Thus transforming  $\vec{c}$  to  $\vec{b} - \vec{c}$  will not change the cell edge lengths. In this case,  $g_1$ ,  $g_2$ , and  $g_3$  are, of course, unchanged and

$$\begin{aligned} g'_4 &= 2\vec{b} \cdot (\vec{b} - \vec{c}) = 2\vec{b} \cdot \vec{b} - 2\vec{b} \cdot \vec{c} = 2g_2 - g_4 = g_4 \\ g'_5 &= 2\vec{a} \cdot (\vec{b} - \vec{c}) = 2\vec{a} \cdot \vec{b} - 2\vec{a} \cdot \vec{c} = g_6 - g_5 \\ g'_6 &= 2\vec{a} \cdot \vec{b} = g_6 \end{aligned}$$

This shows that a single element of  $g_{\{4,5,6\}}$ ,  $g_5$ , will change sign depending on the sign of  $g_6 - g_5$ . Cases 6 and 7 cannot start from the all-obtuse case because  $g_4 = g_2$  and because  $g_2$  must be nonnegative. Starting from an all acute case,  $+++$ , we will remain in the all acute case if  $g_6$  is greater than or equal to  $g_5$  but go to one having one obtuse angle (not reduced) if  $g_6$  is less than  $g_5$ . We then change to having all obtuse angles,  $---$ , by reversing the direction of  $b$ . The resulting matrices in these face-diagonal cases are:

Case 6:  $g_2 = g_4$ ,  $g_5 \geq g_6$ ,  $\vec{a} \rightarrow \vec{a}$ ,  $\vec{b} \rightarrow -\vec{b}$ ,  $\vec{c} \rightarrow \vec{b} - \vec{c}$

$$M_6 = (100000/010000/011\bar{1}00/0\bar{2}0100/0000\bar{1}1/00000\bar{1})$$

$$P_6 = \left( 100000/0\frac{1}{2}0\frac{1}{2}00/001000/0\frac{1}{2}0\frac{1}{2}00/000010/000001 \right)$$

$\mathcal{G}^6$  subspace:  $(r, s, t, s, u + v, v)$

Case 7:  $g_2 = g_4$ ,  $g_5 < g_6$ ,  $\vec{a} \rightarrow -\vec{a}$ ,  $\vec{b} \rightarrow -\vec{b}$ ,  $\vec{c} \rightarrow \vec{c} - \vec{b}$

$$M_7 = (100000/010000/011\bar{1}00/020\bar{1}00/0000\bar{1}1/000001)$$

$$P_7 = \left( 100000/0\frac{1}{2}0\frac{1}{2}00/001000/0\frac{1}{2}0\frac{1}{2}00/000010/000001 \right)$$

$\mathcal{G}^6$  subspace:  $(r, s, t, s, u, u + v)$

Case 8:  $g_2 = -g_4$ ,  $\vec{a} \rightarrow \vec{a}$ ,  $\vec{b} \rightarrow -\vec{b}$ ,  $\vec{c} \rightarrow -\vec{b} - \vec{c}$

$$M_8 = (100000/010000/011100/020100/0000\bar{1}\bar{1}/00000\bar{1})$$

$$P_8 = \left( 100000/0\frac{1}{2}0\frac{1}{2}00/001000/0\frac{1}{2}0\frac{1}{2}00/000010/000001 \right)$$

$\mathcal{G}^6$  subspace:  $(r, s, t, -s, -u, -v)$

Case 9:  $g_1 = g_5$ ,  $g_4 \geq g_6$ ,  $\vec{a} \rightarrow -\vec{a}$ ,  $\vec{b} \rightarrow \vec{b}$ ,  $\vec{c} \rightarrow \vec{a} - \vec{c}$

$$M_9 = (100000/010000/1010\bar{1}0/000\bar{1}01/\bar{2}00010/00000\bar{1})$$

$$P_9 = \left( \frac{1}{2}000\frac{1}{2}0/010000/001000/000100/\frac{1}{2}000\frac{1}{2}0/000001 \right)$$

$\mathcal{G}^6$  subspace:  $(r, s, t, u + v, r, u)$

Case A:  $g_1 = g_5$ ,  $g_4 < g_6$ ,  $\vec{a} \rightarrow -\vec{a}$ ,  $\vec{b} \rightarrow -\vec{b}$ ,  $\vec{c} \rightarrow -\vec{a} + \vec{c}$

$$M_A = (100000/010000/1010\bar{1}0/000\bar{1}01/2000\bar{1}0/000001)$$

$$P_A = \left( \frac{1}{2}000\frac{1}{2}0/010000/001000/000100/\frac{1}{2}000\frac{1}{2}0/000001 \right)$$

$\mathcal{G}^6$  subspace:  $(r, s, t, u, r, u + v)$

Case B:  $g_1 = -g_5$ ,  $\vec{a} \rightarrow -\vec{a}$ ,  $\vec{b} \rightarrow \vec{b}$ ,  $\vec{c} \rightarrow -\vec{a} - \vec{c}$

$$M_B = (100000/010000/101010/000\bar{1}0\bar{1}/200010/00000\bar{1})$$

$$P_B = \left( \frac{1}{2}000\frac{\bar{1}}{2}0/010000/001000/000100/\frac{\bar{1}}{2}000\frac{1}{2}0/000001 \right)$$

$\mathcal{G}^6$  subspace:  $(r, s, t, -u, -r, -v)$

Case C:  $g_1 = g_6, g_4 \geq g_5$ ,  $\vec{a} \rightarrow -\vec{a}$ ,  $\vec{b} \rightarrow \vec{a} - \vec{b}$ ,  $\vec{c} \rightarrow \vec{c}$

$$M_C = (100000/11000\bar{1}/001000/000\bar{1}10/0000\bar{1}0/\bar{2}00001)$$

$$P_C = \left( \frac{1}{2}0000\frac{1}{2}/010000/001000/000100/000010/\frac{1}{2}0000\frac{1}{2} \right)$$

$\mathcal{G}^6$  subspace:  $(r, s, t, u + v, v, r)$

Case D:  $g_1 = g_6$ ,  $g_4 < g_5$ ,  $\vec{a} \rightarrow -\vec{a}$ ,  $\vec{b} \rightarrow -\vec{a} + \vec{b}$ ,  $\vec{c} \rightarrow -\vec{c}$

$$M_D = (100000/11000\bar{1}/001000/000\bar{1}10/000010/20000\bar{1})$$

$$P_D = \left( \frac{1}{2}0000\frac{1}{2}/010000/001000/000100/000010/\frac{1}{2}0000\frac{1}{2} \right)$$

$\mathcal{G}^6$  subspace:  $(r, s, t, u, u + v, r)$

Case E:  $g_1 = -g_6$ ,  $\vec{a} \rightarrow -\vec{a}$ ,  $\vec{b} \rightarrow -\vec{a} - \vec{b}$ ,  $\vec{c} \rightarrow \vec{c}$

$$M_E = (100000/110001/001000/000\bar{1}\bar{1}0/0000\bar{1}0/200001)$$

$$P_E = \left( \frac{1}{2}0000\frac{\bar{1}}{2}/010000/001000/000100/000010/\frac{\bar{1}}{2}0000\frac{1}{2} \right)$$

$\mathcal{G}^6$  subspace:  $(r, s, t, -u, -v, -r)$

The special-position subspaces of the face-diagonal boundary polytopes 6, 8, 9, B, C and E are empty because such a special position would require a common point in the all acute + + + and all obtuse - - - cases that only meet at the axial planes of the  $g_{\{4,5,6\}}$  subspace, which are excluded from the all acute + + + case. For cases 7, A and D there are non-trivial special-position subspaces. An invariant point in case 7 would have to satisfy  $g_5 = g_6 - g_5$  or  $g_5 = g_6/2$ . Thus we define  $7' : \{g_5 = g_6/2\}$  and similarly define  $A' : \{g_4 = g_6/2\}$  and  $D' : \{g_4 = g_5/2\}$ .

#### 6.0.4 Body-diagonal case:

There is only one 5-dimensional body-diagonal case,  $\|\vec{a} + \vec{b} + \vec{c}\| = \|\vec{c}\|$ :

$$\text{Case F: } g_1 + g_2 + g_3 + g_4 + g_5 + g_6 = g_3, \quad \vec{a} \rightarrow -\vec{a}, \quad \vec{b} \rightarrow -\vec{b}, \quad \vec{c} \rightarrow \vec{a} + \vec{b} + \vec{c}$$

$$M_F = (100000/010000/111111/0\bar{2}0\bar{1}0\bar{1}/\bar{2}000\bar{1}\bar{1}/000001)$$

$$P_F = \left( \frac{4\bar{1}\bar{1}}{\bar{5}\bar{5}}0 \frac{\bar{1}\bar{1}\bar{1}}{\bar{5}\bar{5}\bar{5}} / \frac{\bar{1}4}{\bar{5}\bar{5}} \frac{\bar{1}\bar{1}\bar{1}}{\bar{5}\bar{5}\bar{5}} / 001000 / \frac{\bar{1}\bar{1}}{\bar{5}\bar{5}}0 \frac{4\bar{1}\bar{1}}{\bar{5}\bar{5}\bar{5}} / \frac{\bar{1}\bar{1}}{\bar{5}\bar{5}} \frac{\bar{1}4\bar{1}}{\bar{5}\bar{5}\bar{5}} / \frac{\bar{1}\bar{1}}{\bar{5}\bar{5}} \frac{\bar{1}\bar{1}4}{\bar{5}\bar{5}\bar{5}} / \right)$$

$$\mathbf{G}^6 \text{ subspace: } (r, s, t, -u, -v, -r - s + u + v)$$

In order to have a special-position subspace in case F, in addition to  $g_1 + g_2 + g_3 + g_4 + g_5 + g_6 = g_3$ , we need (from the fourth and fifth rows of  $M_F$ ),  $g_4 = -2g_2 - g_4 - g_6$  and  $g_5 = -2g_1 - g_5 - g_6$  from which we have  $2g_2 + 2g_4 = -g_6 = 2g_1 + 2g_5$  from which we take  $F': \{g_1 - g_2 - g_4 + g_5 = 0\}$ . This is equivalent to  $\|\vec{a} + \vec{c}\| = \|\vec{b} + \vec{c}\|$ , *i.e.* that the shorter b-face-diagonal is the same length as the shorter a-face-diagonal.

## 7 The 4-D boundary polytopes

The 4-D boundary polytopes are created by the intersection of 2 5-D boundary polytopes. Certain intersections are degenerate. For example, cases 8, B, E and F are restricted to the  $---$  branch of the boundary of the Niggli cone while cases 6, 7, 9, A, C and D are restricted to the  $+++$  branch. More subtly, cases 6 and 7 require  $g_2 = g_4$ , maximizing  $g_4$ , Forcing  $g_4 \geq g_5$  and  $g_4 \geq g_6$  which would conflict with cases A and D. Only cases 9 and C, respectively, taken to their boundaries with A and D, respectively are possible. Those boundaries are designated 9A and CD, respectively. Similarly, cases 9 and A maximize  $g_5$ , which would conflict with case 7 and force 6 to the 67 boundary, and cases C and D maximize  $g_6$  which would conflict with case 6 except at the 67 boundary. Thus cases 6A, 7A, 6D, 7D, 79, 7A, 6C, 6D actually are the lower dimension cases 69A, 79A, 6CD, 7CD, 79A, 79A, 6CD and 6CD, respectively. This process can result in 3-D or even 2-D boundary polytopes from the intersection of two 5-D boundary polytopes (see below). After excluding the cases that involve any of  $g_{\{1,2,3\}} = 0$ , there are fifty-five 4-D cases as shown in Appendix A Table 7. The relative populations for all the 2-D boundary polytopes except 26, 28, 2A and 2D have Z-scores above -1. The Z-scores for those 4 cases range from -1.1 down to -1.9. (See the supplementary materials A for a discussion of Z-scores).

The edges of the 5-D polytopes can be read directly from Appendix A Table 7. For example the 6 polytope is bounded by 16, 26, 56, 67 and 69 and the F polytope is bounded by 1F, 2F, 8F, BF and EF. It is important to note that the polytopes 1, 2, 3, 4 and 5 extend into the boundaries of both the  $+++$  and  $---$  branches of  $\mathbf{N}$ . Even though the polytopes 3, 4 and 5 do not contain any valid Niggli reduced  $+++$  cells, they are part of both branches of  $\partial(\mathbf{N})$  even for  $+++$ .

## 8 The 3-D boundary polytopes

The 3-D boundary polytopes are created by the intersection of 3 5-D boundary polytopes. In some cases the boundary polytope is better represented by a 4-fold intersection. The boundary polytope 34CD is equivalent to 34C and 34D, 359A is equivalent to 359 and 35A, 4567 is equivalent to 456 and 457, 679C is equivalent to 69C and 79C, and 9ACD is equivalent to 9AD and ACD. These are “flat boundary intersection” cases in which one side of the flat boundary

intersection implies the other. On the other hand 126 and 127, 12A and 129, 12C and 12D, 2AD and 29C, 69C and 79C are distinct rather than equivalent pairs of flat boundary intersections. Six 2-fold intersections of 5-D boundary polytopes (6A, 6C, 79, 7D, 9D and AC) result in 3-D boundary polytopes, rather than in 4-D boundary polytopes. In each case both boundary polytopes have mismatched partners from “flat boundary intersections”. Let us examine the 6A case in detail, elaborating on the discussion of the 4-D boundary polytopes above.

Cases 6 and A are  $g_2 = g_4$  and  $g_5 \geq g_6$  and  $g_1 = g_5$  and  $g_4 < g_6$ , respectively. For intersections, we use the closures of the boundary polytopes, so we have the closure of A as  $g_1 = g_5$  and  $g_4 \leq g_6$ . The Niggli cone itself imposes the additional restrictions  $g_6 \leq g_1$  and  $g_1 \leq g_2$ , but from 6,  $g_2 = g_4$  and from the closure of A,  $g_4 \leq g_6$ , so we have

$$g_2 = g_4 \leq g_6 \leq g_1 \Rightarrow g_2 \leq g_1$$

and from the Niggli reduction conditions

$$g_1 \leq g_2$$

thus  $g_1 = g_2$  and  $g_4 = g_6$ , meaning that, in addition to satisfying the constraints of case A, we also satisfy the constraints of case 9,  $g_1 = g_5$  and  $g_4 \geq g_6$ . Thus case 6A is actually case 69A, producing a true 3-D boundary polytope from the intersection of 2 5-D boundary polytopes due to the additional constraints of Niggli reduction. As we will see in the discussion of the 2-D boundary polytopes, the Niggli reduction constraints can result in shedding one or more degrees of freedom, allowing some 2-fold intersections of 5-D boundary polytopes to result in 2-D boundary polytopes.

After excluding the cases that involve any of  $g_{\{1,2,3\}} = 0$ , there are seventy-nine cases as shown in Appendix A Table 8. The relative populations for all the 3-D boundary polytopes have Z-scores greater than -1.1.

For completeness, if one wished to include the boundary polytope with  $g_1 = 0$  it would be considered in the 3-D polytopes. In  $cl(\mathbf{N})$ ,  $g_1 = 0$  forces  $g_5 = g_6 = 0$ ,  $g_2 = 0$ , leaving only 3 degrees of freedom at  $\partial(\mathbf{N})$ . Note that  $g_2 = 0$  is of even lower dimension, 1, because  $g_2 = 0$  forces  $g_4 = 0$  as well as  $g_1 = g_5 = g_6 = 0$ , leaving only 1 degree of freedom ( $g_3$ ).  $g_3 = 0$  is just the origin.

## 9 The 2-D boundary polytopes

The 2-D boundary polytopes are, in general, created by the intersection of 4 5-D boundary polytopes, but several well-populated 4-fold intersections result in 3-D boundary polytopes rather than 2-D boundary polytopes. Several 4-fold intersections are most naturally presented as higher multiplicity intersections, and in some cases the intersection of as few as 2 5-D boundary polytopes is sufficient to create a 2-D boundary polytope. After excluding the cases that involve any of  $g_{\{1,2,3\}} = 0$ , there are fifty-five cases as shown Appendix A Table 9. The combination of 7 boundary polytopes 1679ACD is the hexagonal rhombohedral  $hR$ , lattice character 9, Roof/Niggli symbol 49B, subspace  $(r, r, s, r, r, r)$ . Alternatively, lattice character 9 can be viewed as any of 81 other intersections, including 2 2-folds (6D, 7A), 18 3-folds (179, 16A, 16C, 16D, 17A, 17D, 19D, 1AC, 67A, 67D, 69D, 6AC, 6AD, 6CD, 79A, 79D, 7AC, 7AD), 33 4-folds (1679 167A, 167C, 167D, 169A, 169C, 169D, 16AC, 16AD, 16CD, 179A, 179C, 179D, 17AC, 17AD, 17CD, 19AC, 19AD, 19CD, 1ACD, 679A, 679D, 67AC, 67AD, 67CD, 69AC, 69AD, 69CD, 6ACD, 79AC, 79AD, 79CD, 7ACD), 21 5-folds (1679A, 1679C, 1679D, 167AC, 167AD, 167CD, 169AC, 169AD, 169CD, 16ACD, 179AC, 179AD, 179CD, 17ACD, 19ACD, 679AC, 679AD, 679CD, 67ACD, 69ACD, 79ACD) and 7 6-folds (1679AC, 1679AD, 1679CD, 167ACD, 169ACD, 179ACD, 679ACD) and

is a very highly populated 2-D boundary polytope. If we exclude this case, the remaining fifty-four cases have Z-scores ranging from -1.36 (for 1456) to 0.84 (for 123E) to 2.75 (for 29ACD).

Let us consider how one of the 2-folds, 6D, results in only 2-degrees of freedom. Cases 6 and D are  $g_2 = g_4$  and  $g_5 \geq g_6$  and  $g_1 = g_6$  and  $g_4 < g_5$ , respectively. The closure of D is  $g_1 = g_6$  and  $g_4 \leq g_5$ , and Niggli reduction requires  $g_6 \leq g_1 \leq g_2$ , from which it follows that

$$g_6 = g_1 \leq g_2 = g_4 \leq g_5 \leq g_1$$

and therefore

$$g_6 = g_1 = g_2 = g_4 = g_5$$

creating the subspace  $(r, r, s, r, r, r)$ , *i.e.* 2 degrees of freedom.

## 10 The 1-D boundary polytopes

There are 14 distinct 1-D boundary polytopes, with many equivalent presentations. The most complex situation is best presented as an 8-fold intersection, 12679ACD, *i.e.*  $g_1 = g_2 = g_3 = g_4 = g_5 = g_6$ , which is the face-centered cubic  $(r, r, r, r, r, r)$ . There are 81 other equivalent presentations of the face-centered cubic, inherited from the 7-fold intersection hexagonal rhombohedral discussed above by adding case 2 to each of those presentations, thereby providing 2 3-folds for the face centered cubic (26D and 27A). The remaining 13 1-D boundary polytopes are 12345  $(r, r, r, 0, 0, 0)$ , 1234CD  $(r, r, r, 0, 0, r)$  (equivalent to 1234C, 1234D, 123CD, 124CD), 1234E  $(r, r, r, 0, 0, -r)$ , 12359A  $(r, r, r, 0, r, 0)$  (equivalent to 12359, 1235A, 1239A, 1259A), 1235B  $(r, r, r, 0, -r, 0)$ , 123AD  $(r, r, r, 0, r, r)$ , 123BEF  $(r, r, r, 0, -r, -r)$  (equivalent to 123BE, 123BF, 123EF, 12BEF, 23BEF), 124567  $(r, r, r, r, 0, 0)$  (equivalent to 12456, 12457, 12467, 12567), 12458  $(r, r, r, -r, 0, 0)$ , 1247C  $(r, r, r, r, 0, r)$ , 1248EF  $(r, r, r, -r, 0, -r)$  (equivalent to 1248E, 1248F, 124EF, 128EF), 12569  $(r, r, r, r, r, 0)$ , 1258BF  $(r, r, r, -r, -r, 0)$  (equivalent to 1258B, 1258F, 125BF, 128BF).

These 14 1-D boundary polytopes of  $\mathbf{N}$  correspond exactly to the 14 vertices of the hyperpolyhedra in [12, Table 1] for which none of  $g_{\{1,2,3\}}$  are zero. The 14 that match are a confirmation of the completeness of this analysis. Due to the distortion introduced by projection, the rejection of the cases for which any of  $g_{\{1,2,3\}}$  are zero is important in preserving the metric for incommensurate edges near the origin.

If we exclude the highly populated face-centered cubic, the Z-scores for the relative populations of the remaining 13 1-D boundary polytopes range from more than -1.1 for 12569 to 1.44 for 123BEF.

## 11 Relationship between boundary polytopes and lattice-type

“**Lattice characters**” provide a finer-grained division of lattice type than the 14 Bravais lattice types [8, International Tables, Volume A]. In order to understand the relationship among between the 216  $\mathbf{G}^6$  boundary polytopes and the 44 lattice characters in the International Tables, we use combinations of the 15 5-D boundary polytopes and of the special-position subspaces of those polytopes. There are multiple alternate representations of some of the lattice characters. We discuss some of them below.

We refer to Roof’s redrawn Niggli figure identifiers [22] as “**Roof/Niggli symbols**.” We may associate the Roof/Niggli symbols, lattice characters and Bravais lattice types with the

indicated subspaces of  $\mathbf{G}^6$  and combinations of boundary polytopes and special conditions as shown in Tables 2 and 3. The triclinic lattice characters 31 and 44 are not included because no boundary polytopes are needed for the triclinic case as they fill the Niggli-reduced cone.

The primitive Bravais lattice types have a simple relationship to the boundary polytopes. The primitive cubic, which has one degree of freedom as a  $\mathbf{G}^6$  subspace, is the intersection of five 5-D boundary polytopes. The primitive tetragonal and primitive hexagonal lattice types each have two degrees of freedom as  $\mathbf{G}^6$  subspaces and each is the intersection of four 5-D boundary polytopes. The primitive orthorhombic lattice type has three degrees of freedom as a  $\mathbf{G}^6$  subspace and is the intersection of three 5-D boundary polytopes. The primitive monoclinic lattice types each have four degrees of freedom as  $\mathbf{G}^6$  subspaces, and each is the intersection of two 5-D boundary polytopes.

The combination of 8 boundary polytopes 12679ACD (equivalent to the 3-fold combinations 26D and 27A) is the face-centered cubic  $cF$ , lattice character 1, Roof/Niggli symbol 44C, subspace  $(r, r, r, r, r, r)$  [3]. Alternatively,  $cF$  can be viewed as any of  $\hat{1}27$ ,  $\hat{1}2A$  or  $\hat{1}2D$  and of several other intersections. As one would expect from the large number of intersecting boundary polytopes, this is a very complex region of  $\mathbf{G}^6$  and will be the subject of a later paper.

The 1-D combinations of 6 boundary polytopes 1234CD (equivalent to the 5-folds 1234C, 1234D, 123CD, 124CD), 12359A (equivalent to the 5-folds 12359, 1235A, 1239A, 1259A), 123BEF (equivalent to the 5-folds 123BE, 123BF, 123EF, 12BEF, 23BEF), 124567 (equivalent to the 5-folds 12456, 12457, 12467, 12567), 1248EF (equivalent to the 5-folds 1248E, 1248F, 124EF, 128EF), 1258BF (equivalent to the 5-folds 1258B, 1258F, 125BF, 128BF) form the subspaces

$$\begin{aligned} &(r, r, r, 0, 0, r) \\ &(r, r, r, 0, r, 0) \\ &(r, r, r, 0, -r, -r) \\ &(r, r, r, r, 0, 0) \\ &(r, r, r, -r, 0, -r) \\ &(r, r, r, -r, -r, 0) \end{aligned}$$

of which none are Niggli-reduced and are therefore a set of open boundary polytopes.

Most of the 216  $\mathbf{G}^6$  boundary polytopes are non-Niggli-reduced open boundary polytopes of the Niggli region. Therefore only two of the 5-fold boundary polytopes, five of the 4-fold boundary polytopes, eight of the 3-fold boundary polytopes and eleven of the 2-fold boundary polytopes correspond directly to lattice characters. None of the single 5-D boundary polytopes corresponds to lattice characters.

We are working from the boundary polytopes, looking for the resulting symmetries. Hosoya [14] started, instead, from the three highest symmetry lattice types (the three cubics) and added the lower symmetry primitive hexagonal lattice type, and inferred boundary polytopes from the symmetries, having to treat open boundary polytopes as if they were Niggli-reduced. The resulting six boundary polytopes of the three cubics and the primitive hexagonal restated in terms of  $\mathbf{G}^6$  are given in Table 4.

## 12 Summary and Conclusions

The wide-spread use of Niggli reduction in crystallography implies that it should be thoroughly understood. Robust identification of Bravais lattices and lookup of unit cell parameters in databases would be improved if a successful embedding of the Niggli space could be achieved. We have investigated and enumerated the several kinds of boundary polytopes on the Niggli cone and enumerated the transformations and projectors specific to each. While other, related,

work has often used 3-D sections, our work natively addresses the boundary polytopes and transformations in the Euclidean space  $\mathbf{G}^6$ . The single point of view and the simple linear algebra involved makes the presentation more consistent.

Some unexpected complexities have been encountered, such as the occurrence of one boundary polytope that is the intersection of eight 5-D boundary polytopes, a fruitful area for further investigation.

## Acknowledgement

The authors acknowledge the invaluable assistance of Frances C. Bernstein.

The work by Herbert J. Bernstein has been supported in part by NIH NIGMS grant 2R15GM078077-02. The content is solely the responsibility of the authors and does not necessarily represent the official views of the funding agency.

The authors wish to thank the referee who caught some errors in the dimensions assigned to some of the boundary polytopes in an earlier draft of this paper. The necessary recheck produced one additional boundary polytope, and was the inspiration for the discussion of the reduction in the number of degrees of freedom for some of the 2-folds and 3-folds.

Table 1: Fifteen 5-D boundary polytopes on Niggli-reduced cells in  $\mathbf{G}^6$ . The special-position subspaces are identified by the conditions to be added to the conditions that define the boundary polytope itself. For a given boundary polytope  $\mathbf{I}$ , the column “Condition” gives the  $\mathbf{G}^6$  constraints (prior to closure) of the boundary polytope. When taken with the “Special-Position Subspace” constraint in the last column, the result is the entirety of the special-position subspace  $\hat{\mathbf{I}}$ . The “Special-Position Subspace” constraint by itself is  $\mathbf{I}'$ . Boundary polytopes 1 and 2 apply in both the all acute (+ + +) and all obtuse (− − −) branches of the Niggli-reduced cone. Boundary polytopes 8, B, E and F are restricted to the all obtuse (− − −) branch of the Niggli-reduced cone,  $\mathbf{N}$ . Boundary polytopes 6, 7, 9, A, C and D are restricted to the all acute (+ + +) branch of  $\mathbf{N}$ . While the boundary polytopes 3, 4 and 5 are boundaries of both the all acute (+ + +) and all obtuse (− − −) branches, the common special position subspace of those polytopes is just  $g_4 = g_5 = g_6 = 0$  which is part of the (− − −) branch.

Class	Case	Condition	Special-Position Subspace
Equal cell edges	1	$g_1 = g_2$	$g_4 = g_5$
	2	$g_2 = g_3$	$g_5 = g_6$
Ninety degrees	3	$g_4 = 0$	$g_5 = g_6 = 0$
	4	$g_5 = 0$	$g_4 = g_6 = 0$
	5	$g_6 = 0$	$g_4 = g_5 = 0$
Face diagonal	6	$g_2 = g_4$ and $g_5 \geq g_6$	(none)
	7	$g_2 = g_4$ and $g_5 < g_6$	$g_5 = g_6/2$
	8	$g_2 = -g_4$	(none)
	9	$g_1 = g_5$ and $g_4 \geq g_6$	(none)
	A	$g_1 = g_5$ and $g_4 < g_6$	$g_4 = g_6/2$
	B	$g_1 = -g_5$	(none)
	C	$g_1 = g_6$ and $g_4 \geq g_5$	(none)
	D	$g_1 = g_6$ and $g_4 < g_5$	$g_4 = g_5/2$
E	$g_1 = -g_6$	(none)	
Body diagonal	F	$g_1 + g_2 + g_3 + g_4 + g_5 + g_6 = g_3$	$g_1 - g_2 - g_4 + g_5 = 0$

## References

- [1] L. C. Andrews and H. J. Bernstein. The squared power method to fit a plane to a set of points. *Acta Crystallogr.*, A32:504 – 506, 1976.
- [2] L. C. Andrews, H. J. Bernstein, and G. A. Pelletier. A perturbation stable cell comparison technique. *Acta Crystallogr.*, A36:248 – 252, 1980.
- [3] Lawrence C. Andrews and Herbert J. Bernstein. Lattices and reduced cells as points in 6-space and selection of Bravais lattice type by projections. *Acta Crystallogr.*, A44:1009–1018, 1988.
- [4] Lawrence C Andrews and Herbert J Bernstein. The geometry of niggli reduction ii: Bgaol–embedding niggli reduction. *arXiv preprint arXiv:1305.6561*, 2013. <http://arxiv.org/abs/1305.6561>.
- [5] L. V. Azaroff and M. J. Buerger. *The powder method in X-ray crystallography*, chapter Chapter 11, Reduced cells and their application, pages 124 – 159. McGraw-Hill, 1958.



Table 2: Roof/Niggli symbol, International Tables (IT) lattice character, Bravais lattice type,  $G^6$  subspace [3],  $G^6$  boundary polytope.

Roof/ Niggli Symbol	IT Lattice Char	Bravais Lattice Type	$G^6$ Subspace	$G^6$ Boundary Polytope
44A	3	<b>cP</b>	$(r, r, r, 0, 0, 0)$	$12345 = 12\hat{3} = 12\hat{4} = 12\hat{5}$
44C	1	<i>cF</i>	$(r, r, r, r, r, r)$	12679ACD
44B	5	<i>cI</i>	$(r, r, r, -2r/3, -2r/3, -2r/3)$	$12F2'F' = 12\hat{F}$
45A	11	<b>tP</b>	$(r, r, s, 0, 0, 0)$	$1345 = 1\hat{3} = 1\hat{4} = 1\hat{5}$
45B	21	<b>tP</b>	$(r, s, s, 0, 0, 0)$	$2345 = 2\hat{3} = 2\hat{4} = 2\hat{5}$
45D	6	<i>tI</i>	$(r, r, r, -r + s, -r + s, -2s)$	$12FF' = 12\hat{F}$
45D	7	<i>tI</i>	$(r, r, r, -2s, -r + s, -r + s)$	$12F2' = 12\hat{F}$
45C	15	<i>tI</i>	$(r, r, s, -r, -r, 0)$	158BF
45E	18	<i>tI</i>	$(r, s, s, r/2, r, r)$	$2ADA' = 2\hat{A}D$
48A	12	<b>hP</b>	$(r, r, s, 0, 0, -r)$	134E
48B	22	<b>hP</b>	$(r, s, s, -s, 0, 0)$	2458
49C	2	<i>hR</i>	$(r, r, r, s, s, s)$	$121'2' = 1\hat{2}$
49D	4	<i>hR</i>	$(r, r, r, -s, -s, -s)$	$121'2' = 1\hat{2}$
49B	9	<i>hR</i>	$(r, r, s, r, r, r)$	1679ACD
49E	24	<i>hR</i>	$(r, s, s, -s + r/3, -2r/3, -2r/3)$	$2F2'F' = 2\hat{F}$
50C	32	<b>oP</b>	$(r, s, t, 0, 0, 0)$	$345 = \hat{3} = \hat{4} = \hat{5}$
50D	13	<i>oC</i>	$(r, r, s, 0, 0, -t)$	134
50E	23	<i>oC</i>	$(r, s, s, -t, 0, 0)$	245
50A	36	<i>oC</i>	$(r, s, t, 0, -r, 0)$	35B
50B	38	<i>oC</i>	$(r, s, t, 0, 0, -r)$	34E
50F	40	<i>oC</i>	$(r, s, t, -s, 0, 0)$	458
51A	16	<i>oF</i>	$(r, r, s, -t, -t, -2r + 2t)$	$1F1' = 1\hat{F}$
51B	26	<i>oF</i>	$(r, s, t, r/2, r, r)$	$ADA' = \hat{A}D$
52A	8	<i>oI</i>	$(r, r, r, -s, -t, -2r + s + t)$	12F
52B	19	<i>oI</i>	$(r, s, s, t, r, r)$	$29C = 2AD$
52C	42	<i>oI</i>	$(r, s, t, -s, -r, 0)$	58BF

Table 3: Roof/Niggli symbol, International Tables (IT) lattice character, Bravais lattice type,  $G^6$  subspace,  $G^6$  boundary polytope, continued

Roof/ Niggli Symbol	IT Lattice Char	Bravais Lattice Type	$G^6$ Subspace	$G^6$ Boundary Polytope
53A	33	<b>mP</b>	$(r, s, t, 0, -u, 0)$	35
53B	35	<b>mP</b>	$(r, s, t, -u, 0, 0)$	45
53C	34	<b>mP</b>	$(r, s, t, 0, 0, -u)$	34
55A	10	<i>mC</i>	$(r, r, s, t, t, u)$	$11' = \hat{1}$
55A	14	<i>mC</i>	$(r, r, s, t, t, u)$	$11' = \hat{1}$
57B	17	<i>mC</i>	$(r, r, s, -t, -u, -2r + t + u)$	1F
55B	20	<i>mC</i>	$(r, s, s, t, u, u)$	$22' = \hat{2}$
55B	25	<i>mC</i>	$(r, s, s, t, u, u)$	$22' = \hat{2}$
57C	27	<i>mC</i>	$(r, s, t, u, r, r)$	9C = AD
56A	28	<i>mC</i>	$(r, s, t, u, r, 2u)$	$AA' = \hat{A}$
56C	29	<i>mC</i>	$(r, s, t, u, 2u, r)$	$DD' = \hat{D}$
56B	30	<i>mC</i>	$(r, s, t, s, u, 2u)$	$77' = \hat{7}$
54C	37	<i>mC</i>	$(r, s, t, -u, -r, 0)$	5B
54A	39	<i>mC</i>	$(r, s, t, -u, 0, -r)$	4E
54B	41	<i>mC</i>	$(r, s, t, -s, -u, 0)$	58
57A	43	<i>mC</i>	$(r, s, t, -s + u, -r + u, -2u)$	$FF' = \hat{F}$

Table 4: The Hosoya boundary polytopes of the three cubic lattice types and the primitive hexagonal in terms of  $G^6$

<i>Hosoya</i> <sub>1</sub>	$2g_1 = g_5 + g_6$
<i>Hosoya</i> <sub>2</sub>	$2g_2 = g_4 + g_6$
<i>Hosoya</i> <sub>3</sub>	$2g_3 = g_4 + g_5$
<i>Hosoya</i> <sub>4</sub>	$g_4 = g_5$ , the special-position subspace of case 1
<i>Hosoya</i> <sub>5</sub>	$g_5 = g_6$ , the special-position subspace of case 2
<i>Hosoya</i> <sub>6</sub>	$g_4 = g_5/2$ , the special-position subspace of case D

- [6] E. Beltrami. Sulle funzioni bilineari. *Giornale di Matematiche ad Uso degli Studenti Delle Università*, 11:98 – 106, 1873.
- [7] M. J. Buerger. Note on reduced cells. *Zeitschrift für Kristallographie*, 113:52 – 56, 1960.
- [8] H. Burzlaff, H. Zimmermann, and P. M. de Wolff. *International Tables for Crystallography, Vol. A*, chapter 9. Crystal Lattices, pages 734 – 744. Dordrecht: Kluwer Academic Publishers, 1992.
- [9] S. K. Byram, C. F. Campana, J. Fait, and R. A. Sparks. Using nist crystal data within siemens software for four-circle and smart ccd diffractometers. *Journal of Research - National Institute of Standards and Technology*, 101:295 – 300, 1996.
- [10] B. N. Delaunay. Neue Darstellung der geometrischen Kristallographie. *Zeitschrift für Kristallographie*, 84:109 – 149, 1932.
- [11] B. Gruber. The relationship between reduced cells in a general bravais lattice. *Acta Crystallogr.*, A29:433 – 440, 1973.
- [12] B. Gruber. Classification of lattices: a new step. *Acta Crystallogr.*, A53:505 – 521, 1997.
- [13] B. Gruber. *International Tables for Crystallography, Vol. A*, chapter 9.3, “Further properties of lattices”, pages 756 – 760. Wiley Online Library, 2006.
- [14] M. Hosoya. The least set of conditions to specify a bravais lattice uniquely in its parameter space. *Bulletin of the College of Science. University of the Ryukyus*, 50:1 – 13, 1990.
- [15] M. Hosoya. A finite group that derives all the 14 Bravais lattices as its subgroups. *Acta Crystallographica*, A56(3):259–263, 2000.
- [16] C. Jordan. Mémoire sur les formes bilinéaires. *Journal de Mathématiques Pures et Appliquées, deuxième Série*, 19:35 – 54, 1874.
- [17] J. Macíček and A. Yordanov. BLAF-a robust program for tracking out admissible Bravais lattice (s) from the experimental unit-cell data. *J. Appl. Crystallogr.*, 25:73 – 80, 1992.
- [18] Keith J McGill, Mojgan Asadi, Maria Toneva Karakasheva, Lawrence C Andrews, and Herbert J Bernstein. The geometry of niggli reduction iii: Sauc-search of alternate unit cells. *arXiv preprint arXiv:1307.1811*, 2013. <http://arxiv.org/abs/1307.1811>.
- [19] W. Minor and Z. Otwinowski. Advances in accuracy and automation of data collection and processing. In *Proceedings of the IUCr computing school*, 1997.
- [20] P. Niggli. *Krystallographische und Strukturtheoretische Grundbegriffe, Handbuch der Experimentalphysik, Vol. 7, part 1*. Akademische Verlagsgesellschaft, Leipzig, 1928.
- [21] R. Oishi-Tomiyasu. Rapid Bravais-lattice determination algorithm for lattice parameters containing large observation errors. *Acta Crystallographica*, A68(5):525–535, 2012.
- [22] R. B. Jr. Roof. Theoretical extension of the reduced-cell concept in crystallography. Technical Report LA-4038, TID-4500, Los Alamos Scientific Lab., NM, 1967. <http://lib-www.lanl.gov/cgi-bin/getfile?00378045.pdf>.
- [23] L. A. Seeber. *Untersuchungen über die Eigenschaften der positiven ternären quadratischen Formen*, volume 1 of *Mathematische Abhandlungen von Ludwig August Seeber*. Tobais Loeffler, Mannheim, 1831.

- [24] E. Selling. Über die binären und ternären quadratischen Formen. *Journal für die reine und angewandte Mathematik (Crelle's Journal)*, 1874(77):143 – 229, 1874.
- [25] G. W. Stewart. On the early history of the singular value decomposition. *SIAM Review*, pages 551 – 566, 1993.
- [26] B. Toby. Private Communication, 1994.
- [27] H. Zimmermann and H. Burzlaff. DELOS A computer program for the determination of a unique conventional cell. *Zeitschrift für Kristallographie*, 170:241 – 246, 1985.

## A Supplementary Materials – The Monte Carlo Search for Boundary Polytopes

One can follow an entirely algebraic process to identify all boundary polytopes. In view of the complexity of the space it is helpful to, use a computer to explore  $\mathbf{N}$  especially to confirm information on the dimensionality of boundary polytopes and on the necessary boundary transformations.

In order to reduce the computational burden and deal with the open boundary polytopes, rather than randomly generating points in  $\mathbf{G}^6$ , we generate random short lines in  $\mathbf{G}^6$  and look for cases in which the boundary of  $\mathbf{N}$  must have been crossed because one end of the line is Niggli-reduced, while the other end is not. The process for the initial search for 5-D boundary polytopes is given in Table 5.

The search for the boundary polytopes resulting from the process in Table 5 produces transformations in the course of Niggli reduction (step 6). We sort the Niggli-reduced  $\mathbf{G}^6$  vectors by the associated transformation matrix from step 6. A high population for a given matrix indicates a significant volume of  $\mathbf{G}^6$  with access to the associated boundary polytope, implying a 5-D boundary polytope (See Fig. 1 and Fig. 2). A lower population for a given matrix possibly implies a lower-dimensional boundary polytope, a common “edge” resulting from the intersection of multiple 5-D boundary polytopes. With enough probes, many of the lower dimensional boundary polytopes can be discovered, but only with difficulty because the information on those lower-dimensional boundary polytopes is swamped in a sea of data about the 5-D boundary polytopes.

Efficient discovery of all these intersections of multiple 5-D boundary polytopes requires the use of “**projectors**”. A projector for a subspace  $\mathbf{Q}$  in  $\mathbf{G}^6$  is a symmetric matrix,  $P$ , that when applied to any point  $\vec{j}$  in  $\mathbf{G}^6$  is such that  $P\vec{j}$  is the closest point in  $\mathbf{Q}$  to  $\vec{j}$ . A projector has the nice property that  $PP = P$ , i.e. that it acts like the identity matrix on the subspace  $\mathbf{Q}$ .

The projector for a given boundary polytope can be discovered by examining the set of Niggli-reduced  $\mathbf{G}^6$  vectors associated with the transform matrix for that boundary polytope. The examination can either be a simple inspection of the list of vectors or can be done algorithmically by use of a singular value decomposition (SVD) calculation [6, 16, 25]. It should be noted that the projector projects onto the hyperplane associated with the polytope and may project a point from  $\mathbf{G}^6$ , or even from  $\mathbf{N}$  itself, outside of  $\mathbf{N}$ .

Let us first derive projectors by simple inspection. A search for points near a boundary produces a list of vectors that can be examined for the conditions that are met. For instance, the trial vectors:

4.41605	<b>53.21164</b>	<b>53.3171</b>	-9.85206	-2.73956	-1.78806
4.95245	<b>106.2402</b>	<b>106.5968</b>	-72.3608	-0.26549	-4.79911
5.62821	<b>98.26772</b>	<b>98.36612</b>	24.37056	1.57819	1.85157

are seen to meet the condition  $g_2 = g_3$ .

The trial vectors:

4.85822	9.79018	40.14963	-3.6758	<b>-0.01092</b>	-2.18456
4.89205	21.22063	75.92303	6.01777	<b>0.05752</b>	2.78514
5.03365	26.32789	46.84058	-17.2646	<b>-0.01252</b>	-2.03757

are seen to meet the condition  $g_5 = 0$ .

In each case the necessary projector is obvious (see projectors  $P_2$  and  $P_3$ , below). In other cases, such as the body-diagonal boundary polytope, or many of the lower-dimensional boundary polytopes involving multiple face-diagonals, simple inspection is challenging. Given a sufficient number of vectors, the projector may be recovered algorithmically from such a list of vectors, rather than by inspection. If a singular value decomposition is done on a list of vectors near to and covering a single 5-D boundary polytope, the vector corresponding to the smallest singular value is the unit normal to that boundary polytope, and the projector onto that polytope is simply the identity minus the projector onto the line of the normal. The projector onto the line of the unit normal is generated by forming a matrix,  $A$ , whose first row is the unit normal and whose remaining rows are set to zero. Then  $A^T A$  is the projector onto the line of that unit normal.

In the general case of a lower-dimensional boundary polytope, the projector onto the boundary polytope is the identity minus the projector  $Q$  onto the hyperplane  $\Omega$  orthogonal to the boundary polytope. In that case a singular value decomposition on the list of vectors near to and covering the lower-dimensional boundary polytope will have small singular values for the vectors spanning  $\Omega$ . The projector  $Q$  onto  $\Omega$  is generated by forming a matrix  $A$  with initial rows consisting of the vectors corresponding to the small singular values and the remaining rows set to zero. Then  $A^T A$  is the projector onto  $\Omega$  and  $I - A^T A$  is the projector onto the boundary polytope.

Once we have found the projectors for the 5-D boundary polytopes, the projectors for their intersections may be generated from their products. The product of two different projectors is not, itself, likely to be a projector, but repeated squaring of that product rapidly converges to the correct projector [1]. Given these projectors, the process for the remaining boundary polytopes is given in Table 6. This process is similar to the initial process, but three new steps have been added: In step 0 the projector for a particular boundary polytope is read in. In step 2A the vector confirmed by step 2 is projected onto the hyperplane containing the boundary polytope, and step 2B verifies that the projected vector is still a valid unit cell. When doing a random perturbation of a vector already projected onto the hyperplane containing a boundary polytope while looking for intersections with that boundary polytope, it is sufficient to use a random vector projected onto that the hyperplane containing the boundary polytope. However, that risks missing some very low dimension cases. That search produced 215 distinct boundary polytopes. The search was then redone, stepping back into the Niggli cone after each projection, and using a full 6-D spherical random search to ensure catching any nearby boundary polytopes. That search added one more distinct boundary polytope, for a total of 216 boundary polytopes.

The dimension of a boundary polytope can be determined by computing the number of eigenvalues equal to 1 of the projector onto the hyperplane containing the boundary polytope, and having distinct boundary projectors is a sufficient condition for two boundary polytopes to be distinct. However, distinct projectors is a necessary, but not sufficient, condition for two boundary polytopes to be distinct, because crossing one bounding hyperplane in two different places can require two different transformation matrices to reduce the result. The reduction transformation matrices themselves are needed to disambiguate cases with the identical bounding hyperplane projector.

In the course of the Monte Carlo investigation of the boundary polytopes resulting from combinations of 5-D boundary polytopes, we track the relative populations as an indicator of a consistent assignment of dimension. The candidates for assignment to a particular dimension are sorted by population, and the list is cut off on a precipitous drop of more than an order of magnitude. For the remaining populations, the mean population  $\mu$  and estimated standard deviation  $\sigma$  are computed. For each population  $\tau$ , a Z-score,  $(\tau - \mu)/\sigma$ , is computed (see [http://en.wikipedia.org/wiki/Standard\\_score](http://en.wikipedia.org/wiki/Standard_score)). Z-scores of less than -1 suggest the possible need for further study of the boundary polytopes involved. A combination of the population analysis resulting from the Monte Carlo search, algebraic analysis of constraints and computation of the eigenvalues of projectors allows the identification of the dimensions of the boundary polytopes, helps to identify distinct combinations of intersections of 5-D boundary polytopes that represent the same lower dimensional boundary polytopes and confirms the critical initial identification of the 15 5-D boundary polytopes identified purely by the Monte Carlo search.

We limit our consideration of valid boundary polytopes to those avoiding the mathematically interesting but crystallographically impossible cases of zero length cell edges. Combinations of boundary polytopes without a valid intersection or with an intersection that would force any of  $g_{\{1,2,3\}}$  to zero or that did not have neighboring Niggli-reduced probe points are eliminated. 574 combinations of 1 through 8 intersecting 5-D boundary polytopes were not degenerate. Many combinations represent equivalent boundary polytopes. There are 216 distinct boundary polytopes. There are 15 5-D boundary polytopes of the full  $G^6$  Niggli cone, 53 4-D boundary polytopes resulting from intersections of pairs of the 15 5-D boundary polytopes, 79 3-D boundary polytopes resulting from the 2-fold and higher intersections of the 15 5-D boundary polytopes, 55 2-D boundary polytopes resulting from 2-fold and higher intersections of the 15 5-D boundary polytopes, 14 1-D boundary polytopes resulting from 3-fold and higher intersections of the 15 5-D boundary polytopes. The ability of the intersection of only 2 5-D boundary polytopes to produce 4-D, 3-D or 2-D boundary polytopes results from the additional constraints imposed by Niggli reduction.

For the 5-D boundary polytopes, three special cases arise in which the Niggli reduction conditions divide a single polytope into two sub-polytopes, the “flat boundary intersections”. In each those three cases, instead of two boundary polytopes meeting at an angle, two boundary polytopes meet edge on. These three cases are  $g_4 = g_2$ ,  $g_5 = g_1$ , and  $g_6 = g_1$ . In each case the division in the polytope is based on the equality of the other two members of  $g_{\{4,5,6\}}$ . For example, when  $g_4 = g_2$ , the division is along  $g_5 = g_6$ . Therefore, when multiplying projectors, instead of multiplying the projector for  $g_4 = g_2$  by itself when the two half-polytopes are required, the second projector is replaced by the projector for the division, *i.e.* in the example given instead of multiplying the projector for  $g_4 = g_2$  by itself, it is multiplied by the projector for  $g_5 = g_6$ .

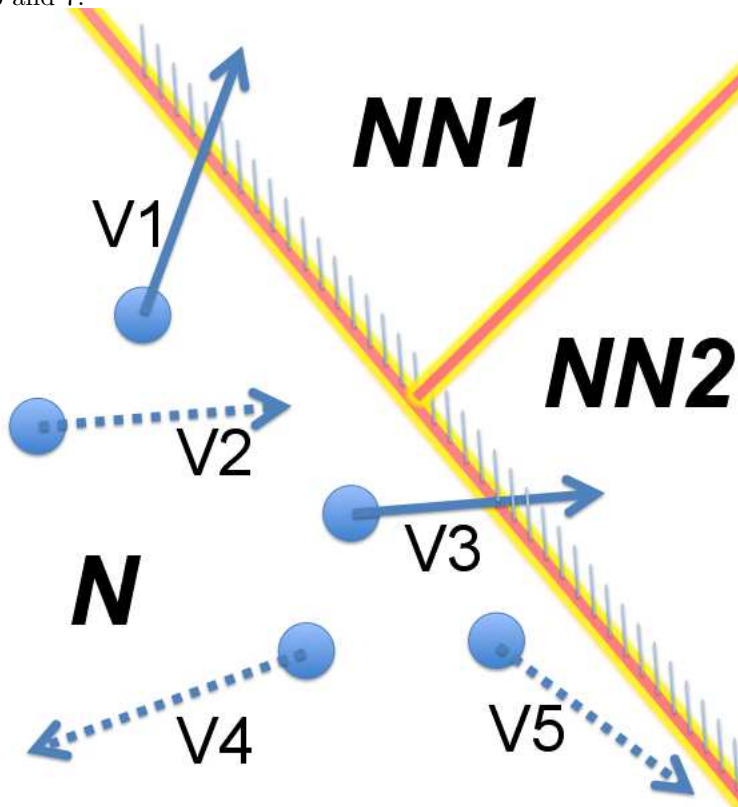
Table 5: Initial process to locate 5-D boundary polytopes

1. Generate a random vector in  $\mathbf{G}^6$ .
2. Confirm that the vector represents a proper unit cell (for instance, the sum of the interaxial angles must be less than 360 degrees).
3. Niggli-reduce the vector.
4. Randomly perturb the vector resulting from step 3.
5. Confirm that the perturbed vector represents a proper unit cell.
6. Niggli-reduce the vector from step 5, accumulating the total transformation matrix from the vector of step 3 to the new reduced vector.
7. If the transformation is the unit matrix, then the perturbed vector was not near the boundary of  $\mathbf{N}$ . Discard the trial. Otherwise, proceed.
8. If the transformation matrix has been discovered before, increment a counter for its occurrences. Otherwise, add it to the list of discovered transformations.
9. Repeat many times, starting at step 1.

Table 6: Process to locate lower-dimensional boundary polytopes.

0. **Read in the projector for the desired boundary to be probed.**
1. Generate a random vector in  $\mathbf{G}^6$ .
2. Confirm that the vector represents a proper unit cell (for instance, the sum of the interaxial angles must be less than 360 degrees).
- 2A. **Project the vector confirmed in step 2 onto the boundary.**
- 2B. **Confirm that the projected vector is still a valid unit cell.**
3. Niggli-reduce the vector.
4. Randomly perturb the vector resulting from step 3.
5. Confirm that the perturbed vector represents a proper unit cell.
6. Niggli-reduce the vector from step 5, accumulating the total transformation matrix from the vector of step 3 to the new reduced vector.
7. If the transformation is the unit matrix, then the perturbed vector was not near the boundary of  $\mathbf{N}$ . Discard the trial. Otherwise, proceed.
8. If the transformation matrix has been discovered before, increment a counter for its occurrences. Otherwise, add it to the list of discovered transformations.
9. Repeat many times, starting at step 1.

Figure 1: Illustration of Monte Carlo search for boundary polytopes in  $\mathbf{G}^6$ . The hatched line represents a boundary polytope, *e.g.*  $g_2 = g_4$ . The unhatched side of the boundary ( $\mathbf{N}$ ) consists of Niggli-reduced cells. In this case the hatched side is divided into two regions,  $\mathbf{NN1}$  (*e.g.*  $g_5 \geq g_6$ ) and  $\mathbf{NN2}$  (*e.g.*  $g_5 < g_6$ ) for which different reduction matrices are required to get a Niggli-reduced cell, *e.g.*  $M_6$  for  $\mathbf{NN1}$  and  $M_7$  for  $\mathbf{NN2}$ . “ $\mathbf{NN}$ ” stands for not Niggli-reduced.  $V1$  is a randomly generated probe point in region  $\mathbf{N}$  for which a random short line reaches across the boundary to reach region  $\mathbf{NN1}$ , so the starting point is associated with  $M_6$ .  $V2$ ,  $V4$  and  $V5$  are randomly generated probe points for which the random short line remains in the Niggli-reduced region  $\mathbf{N}$ . Therefore  $V2$ ,  $V4$  and  $V5$  are discarded.  $V3$  is a randomly generated probe point in region  $\mathbf{N}$  for which a random short line reaches across the boundary to reach region  $\mathbf{NN2}$ , so the starting point is associated with  $M_7$ . Because of this difference in reduction matrices, the boundary polytope is treated as consisting of two distinct boundary polytopes, in this case, cases 6 and 7.





**A SUPPLEMENTARY MATERIALS – THE MONTE CARLO SEARCH FOR  
BOUNDARY POLYTOPES**

---

Figure 2: Counts of points found near various boundary polytopes in 100 million trials, organized in declining order of counts, showing the most populated 23 of the 92 boundary polytopes found in this run. This is a run with no filtering for any particular boundary with the counts shown on a logarithmic scale. Note the precipitous drop of nearly 2 orders of magnitude after the first 15 boundary polytopes. This drop confirms that those 15 boundary polytopes are the 5-D boundary polytopes and that there is a vanishingly small probability of there being any other 5-D boundary polytopes of the Niggli-reduced cells.

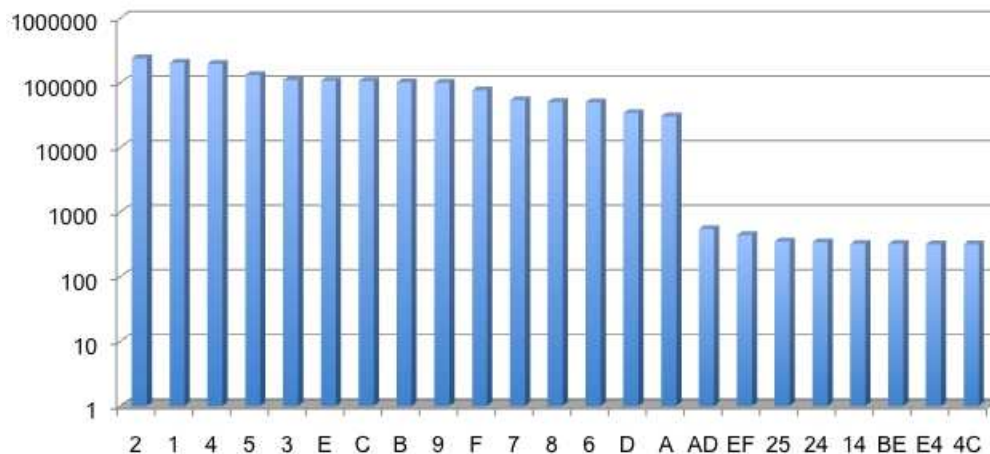


Table 7: The 53 4-D boundary polytopes. The boundary conditions use the symbol notation of Table 1 for the 5-D boundary polytopes. The bounding 4-D polytopes of each of the 15 5-D boundary polytopes can be read off from this table by going down the appropriate column to the main diagonal and then across. For example, the edges of the 3 polytope are 13, 23, 34, 35, 3A, 3B, 3D and 3E.

$g_2 = g_3$	$g_4 = 0$	$g_5 = 0$	$g_6 = 0$	a-face-diagonals	b-face-diagonals	c-face-diagonals	body
12	13 23	14 24	15 25	16 17 18 26 27 28	19 1A 1B 29 2A 2B	1C 1D 1E 2C 2D 2E	1F 2F
		34 45	35 45	47 48 56 58	3A 3B 59 5B	3D 3E 4C 4E	
				67	69	7C	8F
					9A	9C AD BE	BF
						CD	EF

**A SUPPLEMENTARY MATERIALS – THE MONTE CARLO SEARCH FOR  
BOUNDARY POLYTOPES**

---

Table 8: The 79 3-D boundary polytopes. In some cases the most natural presentation of a given 3-D polytope is a 4-fold intersection. In each of those case an equivalent 3-fold intersection is given in parentheses immediately below the 4-fold.

$g_4=0$	$g_5=0$	$g_6=0$	a-face-diagonals			b-face-diagonals			c-face-diagonals			body
123	124 134	125 135 145	126	127	128	129	12A 13A	12B 13B	12C	12D 13D	12E 13E 14E	12F
			156	147 167	148 158	159 169		15B	14C	17C		18F
							19A			1AD		1BF
									1CD			1EF
	234	235 245		247	248		23A	23B	24C	23D	23E 24E	
			256	267	258	259 269		25B	27C			28F
							29A		29C	2AD	2BE	2BF
									2CD			2EF
		345					359A (359)	35B	34CD (34C)		34E	
									3AD		3BE	
			4567 (456)									
				458					47C		48EF (48E)	
						569		58BF (58B)				
						679C (679)						
									9ACD (9AC)			
												BEF

**A SUPPLEMENTARY MATERIALS – THE MONTE CARLO SEARCH FOR  
BOUNDARY POLYTOPES**

---

Table 9: The 55 2-D boundary polytopes

$g_5=0$	$g_6=0$	a-face-diagonals	b-face-diagonals	c-face-diagonals	body
1234	1235 1245	1247 1248 1256 1258 1267	123A 123B 1259 125B 1269 129A	123D 123E 124C 124E 127C 12AD 12CD	128F 12BF 12EF
	1345		134CD (134C) 1359A 135B (1359)	134E 13AD 13BEF (13BE)	
		14567 (1456) 1458		147C 148EF (148E)	
			1569 158BF (158B)		
				1679ACD (6D, 7A)	
	2345		2359A 235B (2359)	234CD 234E (234C) 23AD 23BE	
		24567 (2456) 2458		247C 248EF (248E)	
			2569 258BF (258B)		
			2679C (2679)		
			29ACD (29AC)		
					2BEF